Article

Detection of Reactive Tetrahedral Intermediates in a Deep Cavitand with an Introverted Functionality

Richard J. Hooley, Tetsuo Iwasawa, and Julius Rebek

J. Am. Chem. Soc., **2007**, 129 (49), 15330-15339 • DOI: 10.1021/ja0759343

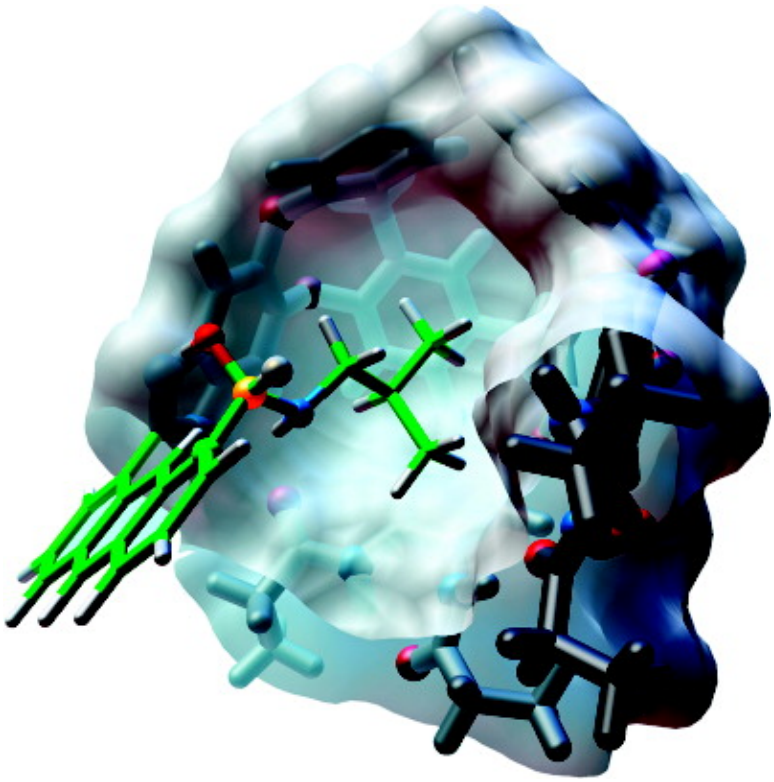

J|A|C|S
ARTICLES
Published on Web 11/16/2007

Detection of Reactive Tetrahedral Intermediates in a Deep Cavitand with an Introverted Functionality

Richard J. Hooley, Tetsuo Iwasawa, and Julius Rebek, Jr.*

Contribution from The Skaggs Institute for Chemical Biology and Department of Chemistry, The Scripps Research Institute, MB-26, 10550 North Torrey Pines Road, La Jolla, California 92037

Received August 7, 2007; E-mail: jrebek@scripps.edu

Abstract: Labile hemiaminal intermediates are stabilized by binding in a deep cavitand with an introverted aldehyde functionality. The aldehyde is attached to the cavitand via an anthracene spacer that rotates rapidly about the cavitand rim. The half-lives of these hemiaminals vary from 30 min to over 100 h at ambient temperature, due to hydrogen bonding with the organized peptide-like framework at the cavitand rim. The intermediates are sufficiently long-lived to allow study by 2D NMR techniques requiring many hours of acquisition time. Mechanistic analysis of the dehydration step shows first-order kinetics. The analogous "extroverted" reaction was also performed, where the addition took place outside the cavitand, displaying standard steady-state kinetics; no hemiaminal was observed. The cavitand shows strong selectivity based not on binding affinity but upon the rate of the product-forming step. A 10:1 ratio of product imines was obtained, while the initial binding ratio was 1:1. The cavitand acts as a mimic of enzymes in that it uses weak binding forces to stabilize reactive intermediates and isolates them from the medium. The synthetic environment allows direct detection and analysis of the intermediates, as opposed to natural systems that must be analyzed indirectly.

Introduction

Some time ago we became involved with synthetic receptors for use in molecular recognition studies. We developed these on the basis of the idea of convergent functional groups; that is, cleft-like structures with inwardly directed functions.[1] They were intended as a complement to the then popular macrocyclics: polyethers for ion recognition,[2] cyclodextrins[3] and synthetic cyclophanes[4] that provided hydrophobic pockets for studies in aqueous solution. Introverted functionality has parallels in natural systems. Binding sites of enzymes and other receptors are created by functional group side chains of the amino acids. A linear structure (polypeptide or RNA strand) can fold around a substrate and more or less completely surround and isolate it; in the folded state the functionality converges on the substrate. Our first success was with the introverted carboxylic acid **1** (Figure 1), a Kemp's triacid[5] fused to a deepened cavitand[6] derived from Högberg's resorcinarene scaffold.[7] This showed the desired recognition and tight binding of amines in either organic[8] or aqueous media.[9] One behavior of this system was nothing short of astonishing: the Menschutkin reaction of amines with a carboxylic methyl ester usually requires forcing conditions, but when performed with quinuclidine on the introverted acid methyl ester, the reaction was over in seconds under ambient conditions.[10] The quinuclidine is presented with the methyl ester whenever it becomes a guest; there are no other choices for the folded state. In other words, the binding and the reaction steps are no longer separate. There have been other examples of synthetic receptors that are able to alter the reactivity of bound species and, in some cases, prolong the lifetimes of otherwise unstable molecules.[11] Examples include the recent isolation of iminium ions[11a] and siloxanes[11c] from a surrounding aqueous environment. Even unfavored conformations of guests[12] and unknown reaction courses[13] can be imposed by the size and shape of the host. Further parallels between this class of synthetic receptors and enzymes have been observed in their activity as catalysts.[14]

(1) Rebek, J., Jr. *Angew. Chem., Int. Ed. Engl.* **1990**, *29*, 245−255.
(2) (a) Cram, D. J. *Science* **1988**, *240*, 760−767. (b) Lehn, J.-M. *Angew. Chem., Int. Ed. Engl.* **1988**, *27*, 89−112.
(3) Breslow, R.; Dong, S. D. *Chem. Rev.* **1998**, *98*, 1997−2011.
(4) (a) Diederich, F. *Angew. Chem., Int. Ed. Engl.* **1988**, *27*, 362−386. (b) Dougherty, D. A.; Stauffer, D. A. *Science* **1990**, *250*, 1558−1560.
(5) Kemp, D. S.; Petrakis, K. S. *J. Org. Chem.* **1981**, *46*, 5140−5143.
(6) Renslo, A. R.; Rebek, J., Jr. *Angew. Chem., Int. Ed.* **2000**, *39*, 3281−3283.
(7) Högberg, A. G. S. *J. Am. Chem. Soc.* **1980**, *102*, 6046−6050.
(8) (a) Wash, P. L.; Renslo, A. R.; Rebek, J., Jr. *Angew. Chem., Int. Ed.* **2000**, *40*, 1221−1222. (b) Iwasawa, T.; Wash, P.L.; Gibson, C.; Rebek, J., Jr. *Tetrahedron* **2007**, *63*, 6506−6511. (c) Renslo, A. R.; Rebek, J., Jr. *Angew. Chem., Int. Ed.* **2000**, *40*, 3281−3283. (d) Park, T. K.; Schroeder, J.; Rebek, J., Jr. *J. Am. Chem. Soc.* **1991**, *113*, 5125−5127.
(9) Butterfield, S. M.; Rebek, J., Jr. *J. Am. Chem. Soc.* **2006**, *128*, 15366−15367.
(10) Purse, B. W.; Ballester, P.; Rebek, J., Jr. *J. Am. Chem. Soc.* **2003**, *125*, 14682−14683.
(11) (a) Dong, V. M.; Fiedler, D.; Carl, B.; Bergman, R. G.; Raymond, K. N. *J. Am. Chem. Soc.* **2006**, *128*, 14464−14465. (b) Ziegler, M.; Brumaghim, J. L.; Raymond, K. N. *Angew. Chem., Int. Ed.* **2000**, *39*, 4119−4121. (c) Yoshizawa, M.; Kusukawa, T.; Fujita, M.; Yamaguchi, K. *J. Am. Chem. Soc.* **2000**, *129*, 6311−6312. (d) Iwasawa, T.; Mann, E.; Rebek, J., Jr. *J. Am. Chem. Soc.* **2006**, *128*, 9308−9309. (e) Kawano, M.; Kobayashi, Y.; Ozeki, T.; Fujita, M. *J. Am. Chem. Soc.* **2006**, *128*, 6558−6559. (f) Fiedler, D.; Bergman, R. G.; Raymond, K. N. *Angew. Chem., Int. Ed.* **2004**, *43*, 6748−6751. (g) Sato, S.; Iida, J.; Suzuki, K.; Ozeki, T.; Fujita, M. *Science* **2007**, *313*, 1273−1276. (h) Murase, T.; Sato, S.; Fujita, M. *Angew. Chem., Int. Ed.* **2007**, *46*, 1083−1085. (i) Chen, J.; Rebek, J., Jr. *Org. Lett.* **2002**, *4*, 327−329.
(12) Scarso, A.; Trembleau, L.; Rebek, J., Jr. *Angew. Chem., Int. Ed.* **2003**, *42*, 5499−5502.
(13) Yoshizawa, M.; Tamura, M.; Fujita, M. *Science* **2006**, *312*, 251−254.

10.1021/ja0759343 CCC: $37.00

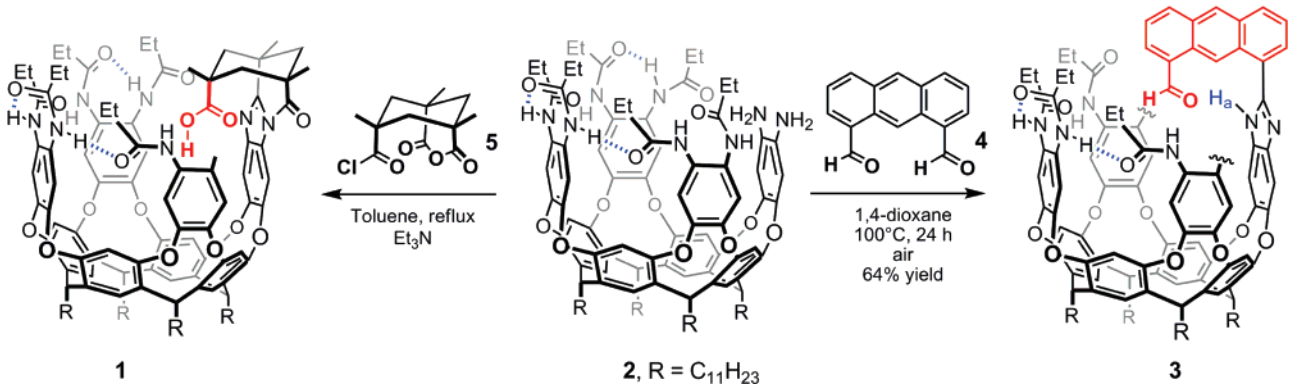

Figure 1. Synthesis of the introverted Kemp's triacid derivative and the introverted aldehyde cavitand **3**. The U-shaped relationship between relevant functions is traced with thickened lines. Some peripheral groups are removed for clarity.

The Kemp's triacid in cavitand **1** is too congested to react with species less reactive than diazoalkanes,[15] and we have now explored other frameworks. The core motif of any inwardly directing group is a 180° relationship between functions, a "U-turn" in the structure, and a 1,8-disubstituted anthracene features this.[16] It also offers the advantage of being functionalizable, so a variety of introverted species can be envisaged. From a synthetic point of view, the easiest group to introvert is an aldehyde, cavitand **3**. Recently we used this species to stabilize tetrahedral intermediates—hemiaminals—in carbonyl addition reactions,[17] and here we report these studies in detail.

The formation of imines via addition of primary amines to aldehydes is a particularly well-studied reaction; indeed, it appears in most undergraduate organic chemistry textbooks.[18] The mechanism is well-known; in nonpolar solvents the reaction proceeds through an intermediate hemiaminal. The process is catalyzed by acids or bases (often the reactants themselves), and the proton transfers involved generate additional, short-lived intermediates. The hemiaminal is—except in very special cases—not observed.[19] It is energetically disfavored, as the breaking of the carbonyl bond and the entropic price of bringing the two reactants together are not always compensated by the new covalent bonds formed. Accordingly, the unstable hemiaminal dissociates to starting materials or proceeds to imine with loss of water. This reaction has been exploited by both chemists and Nature for its high yields and mild conditions. The recent explosion in the study of "organic catalysis" is partly due to the use of imine/enamine-based reactions;[20] in Nature, aldolase enzymes employ imine intermediates.[20] These enzymes stabilize intermediates by providing functional groups that actively lower the energy of a bound transition state, via hydrogen-bonding or other weak intermolecular forces. Detection and analysis of reactive intermediates in biological systems is essential for the accurate determination of enzyme mechanism, but the high activity of enzymes has made such observations difficult. X-ray crystallographic analysis of tetrahedral intermediates inside the active site of D-2-deoxyribose-5-phosphate (DRP) aldolase has been possible at cryogenic temperatures via selective mutation to prevent the enzyme from completing the reaction.[21a] The cavitand is in several ways reminiscent of an enzyme active site, comprising a hydrophobic cavity, an *organized* secondary amide scaffold,[22] and inwardly directed functional groups folded around the substrate. If amines are added to **3**, the system is similar in action to a mutant DRP aldolase in which only the first half of the amine-catalyzed aldol reaction occurs.

Results and Discussion

I. Cavitand Structure. Cavitand **3** was synthesized from the known hexamide-diamine cavitand **2**[6] by condensation with 1,8-anthracenedialdehyde **4** using air as the oxidant.[16,23] The resulting introverted aldehyde shows good solubility in a variety of solvents. The six amide groups at the rim are sufficient to stabilize the folded vase-like conformation, as long as the solvent is a sufficiently good guest for the cavity.[24] In practice, this condition extends to most common aprotic solvents, with the exception of mesitylene-d_{12}, which is too large to bind.[25] The cavitand is nonsymmetric and shows peaks for each proton in its ^{1}H NMR spectrum. The most instructive regions are shown in Figure 2 (see Supporting Information for the complete spectrum). The benzimidazole N*H* appears as a sharp singlet at δ 11.8 ppm, indicative of strong intramolecular H-bonding. Each of the amide N*H*'s appears as a singlet downfield of the aromatic region, and 16 distinct aromatic peaks are seen for the resorcinarene and "wall" protons. Each of the protons on the anthracene ring, including the introverted aldehyde and C*H*, exhibit only one peak. Four of the six methyl groups from the

(14) Hooley, R. J.; Biros, S. M.; Rebek, J. *Angew. Chem., Int. Ed.* **2006**, *45*, 3517−3519.
(15) Purse, B. W.; Rebek, J., Jr. *Proc. Natl. Acad. Sci. U.S.A.* **2006**, *103*, 2530−2534.
(16) Nowick, J. S.; Ballester, P.; Ebmeyer, F.; Rebek, J., Jr. *J. Am. Chem. Soc.* **1990**, *112*, 8902−8906.
(17) Iwasawa, T.; Hooley, R. J.; Rebek, J., Jr. *Science* **2007**, *317*, 493−496.
(18) Anslyn, E. V.; Dougherty, D. A. *Modern Physical Organic Chemistry*; University Science Books: Sausalito, CA, 2006; Chapter 10.
(19) (a) Evans, D. A.; Borg, G.; Scheidt, K. A. *Angew. Chem., Int. Ed.* **2002**, *41*, 3188−3191. (b) Floriani, L.; Marianucci, E.; Todesco, P. E. *J. Chem. Res.* **1984**, 126−127. (c) Chudek, J. A.; Foster, R.; Young, D. *J. Chem. Soc., Perkin Trans. 2* **1985**, 1285−1289.
(20) (a) Taylor, M. S.; Jacobsen, E. N. *Angew. Chem., Int. Ed.* **2006**, *45*, 1520−1543. (b) Dalko, P. I.; Moisan, L. *Angew. Chem., Int. Ed.* **2004**, *43*, 5138−5175. (c) List, B. *Acc. Chem. Res.* **2004**, *37*, 548−557. (d) List, B.; Lerner, R. A.; Barbas, C. F. *J. Am. Chem. Soc.* **2000**, *122*, 2395−2396. (e) Northrup, A. B.; MacMillan, D. W. C. *J. Am. Chem. Soc.* **2002**, *124*, 2458−2460.
(21) (a) Heine, A.; DeSantis, G.; Luz, J. G.; Mitchell, M.; Wong, C.-H.; Wilson, I. A. *Science* **2001**, *294*, 369−374. (b) Lorentzen, E.; Siebers, B.; Hensel, R.; Pohl, E. *Biochemistry* **2005**, *44*, 4222−4229.
(22) (a) Hooley, R. J.; Rebek, J., Jr. *J. Am. Chem. Soc.* **2005**, *127*, 11904−11905. (b) Purse, B. W.; Gissot, A.; Rebek, J. *J. Am. Chem. Soc.* **2005**, *127*, 11222−11223.
(23) Lin, S.; Yang, L. *Tetrahedron Lett.* **2005**, *46*, 4315−4319.
(24) Martin, T.; Obst, U.; Rebek, J., Jr. *Science* **1998**, *281*, 1842−1845.
(25) Chapman, K. T.; Still, W. C. *J. Am. Chem. Soc.* **1989**, *111*, 3075−3077.

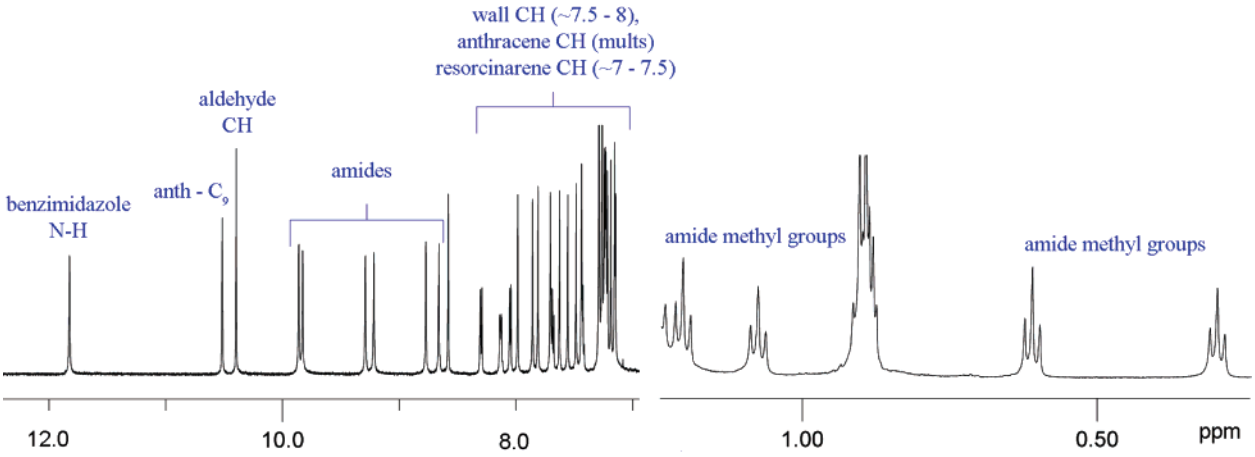

Figure 2. Sections of the ^{1}H NMR spectrum of introverted aldehyde cavitand **3** (600 MHz, $CDCl_3$, 300 K).

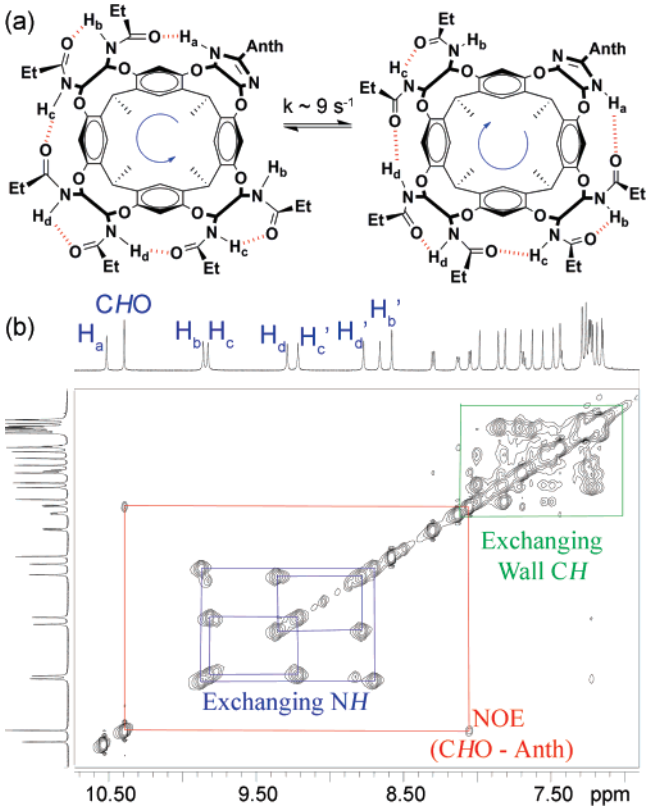

Figure 3. (a) Mechanism of cycloisomerization. (b) Downfield region of the 2D NOESY spectrum of cavitand **3**, showing chemical exchange between amide peaks (600 MHz, $CDCl_3$, 300 ms mixing time).

propionamide rim are visible and are shifted upfield from their usual positions.

There are two possible cycloenantiomeric conformations of the amides at the cavitand rim;[8] the cavitand is chiral but undergoes rapid exchange (on the human time scale) between the two arrays at ambient temperature to yield an overall racemic compound. 2D NOESY analysis of the amide NH region shows chemical exchange cross-peaks between related sets of NH peaks (Figure 3). Integration of these cross-peaks allows an estimation of the rate of interconversion between the two cycloenantiomeric forms.[26] In addition, one set of peaks for exchanging methyl groups is observable (δ 0.6, 0.2) and suitable for calculation. The results (Table 1) show $\Delta G^{\ddagger} \approx 1.5$ kcal mol^{-1}, less than the $\Delta G^{\ddagger}$(rotation) seen for the related octamide cavitand,[27] and are all identical to each other (within error). The lower barrier to exchange seen here can be attributed to the one wall without amide groups; the initial breaking of one hydrogen bond (starting a rotation cascade) becomes easier. The error in $\Delta G^{\ddagger}(H_b)$ is larger due to inaccurate integration caused by overlapping peaks.

Table 1. Barriers to the Cycloisomerization Process in **3**

peaks (δ)	k_1 (s^{-1})	k_{-1} (s^{-1})	$k (=k_1 + k_{-1})$ (s^{-1})	$\Delta G^{\ddagger}$ (kcal mol^{-1})
H_b (9.9, 8.7)	2.7	4.4	7.1	16.4
H_c (9.8, 9.2)	4.5	4.5	9.0	16.2
H_d (9.4, 8.8)	4.7	5.4	10	16.1
Me	4.1	5.1	9.2	16.2

Unlike **1**, cavitand **3** does not have a fixed introverted reactive functionality. The anthracene arm is free to rotate, and so the aldehyde has a choice: it could be introverted, extroverted, or, as we shall soon show, rapidly rotating. To reveal this, the NMR spectra of three cavitands can be compared: aldehyde **3**, imine **6**, and phenyl cavitand **7** (Figure 4). The imine is generated by exposure of **3** to isobutylamine. The substituents of the imine nitrogen are bound inside the cavity; the magnetically shielded environment caused by the cavitand's aromatic rings shifts these signals dramatically upfield. Only one species is seen in the NMR spectrum, indicating that the arm is "locked" over the top of the cavitand, and thus **6** acts as a good model for **3** with the arm in the introverted position. Phenyl cavitand **7** acts as a mimic of "extroverted" **3**; from the cavitand's point of view, the phenyl group is the same as the fixed end of the anthracene. The anthracene arm causes shielding of groups near its aromatic faces, specifically the amide groups on the cavitand rim. The effect of shielding is largest for the imine **6**, as the anthracene is locked over the top of the cavitand, and the amides of the rim are constantly exposed to the extended π surface. For phenyl cavitand **7**, the shielding is negligible. Comparing aldehyde **3** with the two mimics gives a sense of the effects of the anthracene arm when "unlocked" (Figure 4). The amides closest to the benzimidazole in **7** are shifted upfield very slightly from their expected positions, but for the aldehyde **3** and imine **6**, significant upfield shifts occur. This indicates that the arm is

(26) (a) Perrin, C. L.; Dwyer, T. J. *Chem. Rev.* **1990**, *90*, 935−967. (b) Zolnai, Z.; Juranic, N.; Vikic-Topic, D.; Macura, S. *J. Chem. Inf. Comput. Sci.* **2000**, *40*, 611−621.

(27) Rudkevich, D. M.; Hilmersson, G.; Rebek, J., Jr. *J. Am. Chem. Soc.* **1998**, *120*, 12216−12225.

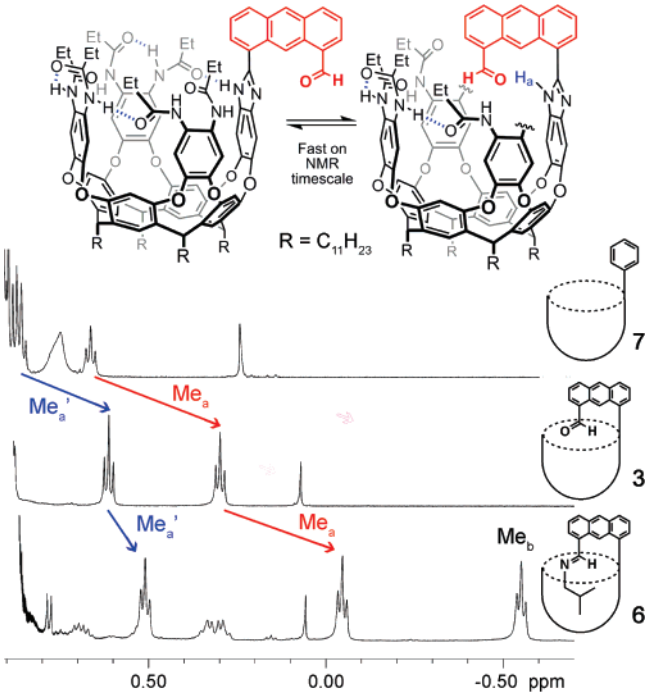

Figure 4. Upfield regions of the ^{1}H NMR spectra (600 MHz, $CDCl_3$, 300 K) of phenyl cavitand **7**, aldehyde **3**, and isobutyl imine **6**, showing the change in chemical shift of the amide rim methyl groups due to shielding by the aromatic arm.

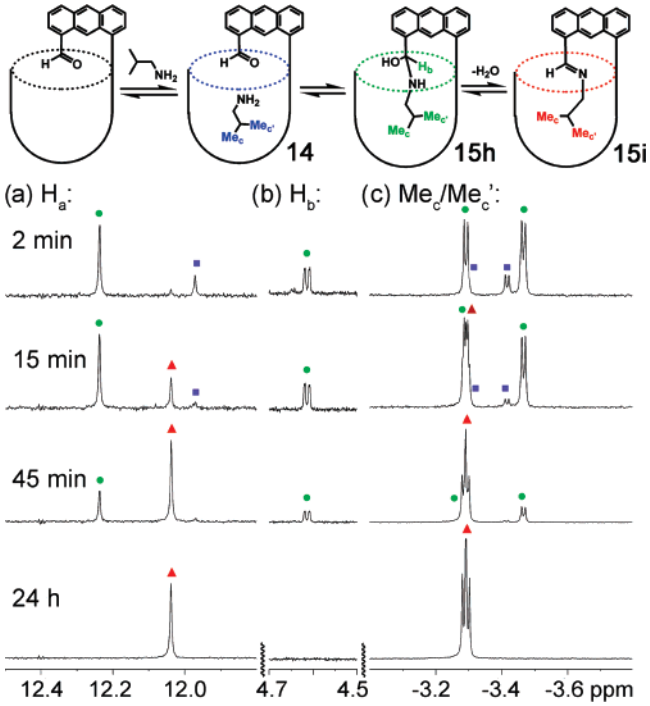

Figure 5. Representation of the reaction process and sections of the ^{1}H NMR spectra obtained upon addition of isobutylamine (10 mM) to a 1.5 mM solution of cavitand **3** in mesitylene-d_{12}. Blue box, host:guest complex **14**; green circle, hemiaminal intermediate **15h**; red triangle, imine product **15i**. (a) Downfield region showing benzimidazole proton H_a (see Figure 2); (b) mid-field region showing hemiaminal CH_b; (c) upfield region showing $Me_{C/C'}$.

rotating rapidly in **3**, as the representative methyl groups are shifted by an amount between the two extreme states of "introverted" mimic **6** and "extroverted" **7**. In imine **6**, the most shifted methyl group does not belong to those closest to the benzimidazole (at the ends of the hexamide chain), but to one—and only one—of the penultimate amides (Me_b, Figure 3). The anthracene arm of the bound imine does not bisect the cavitand but is oriented to one side, shielding one of the exchanging amides significantly more than the other. The assignment of the amides is based on chemical exchange in the 2D NOESY spectrum (see Supporting Information).

II. Stabilization of Reactive Intermediates. The formation of imines is slow enough to monitor conveniently by ^{1}H NMR spectroscopy. As noted previously, cavitand **3** exists in an unfolded (and structurally unknown) state in mesitylene-d_{12} solvent. On addition of a small amine (*n*-propylamine, **8**; isopropylamine, **9**; *n*-butylamine, **10**; isobutylamine, **11**; cyclopropylamine, **12**; or cyclobutylamine, **13**), the cavitand immediately (in 2 min or less) folds into a kinetically stable vase conformation, encapsulating the added amine. The spectra obtained upon addition of isobutylamine are best suited for analysis, so the immediate discussion shall concentrate on those. Within 2 min of mixing, two species are observed, assigned as the noncovalent complex **14** and the corresponding hemiaminal **15h**. The tetrahedral intermediate **15h** gradually undergoes dehydration to the imine product **15i** but, remarkably, is stable enough to be observed *at millimolar concentrations at ambient temperature!* The different complexes display signals for both cavitand and guest with different shifts, leading to rather complex yet interpretable spectra. Figure 5 shows the change in three of these peaks over time; benzimidazole proton H_a (Figure 2) is the most representative cavitand-based signal, as it is distant from the other NH peaks, and its changes are easily visible. The most obvious guest peaks are the terminal CH_3 groups of the amine. The amine methyl groups become diastereotopic due to the chiral cavitand environment when confined inside the cavity (even prior to covalent attachment and hemiaminal formation) and show separate NMR signals. Each complex exhibits two different doublets for these Me groups (the signal for one methyl in noncovalent complex **14** is buried beneath the methyl of the hemiaminal signal at $\delta = -3.29$). The two doublets in imine **15i** are overlapped and appear similar to a triplet.

The pattern of peaks for the reaction of the other amines is similar, but there are notable differences due to the guests' positions inside the cavitand (Figure 6). The $\Delta\delta$ value for the terminal methyl groups gives a good estimate for their position in the cavitand—a CH_3 residing at the base of the cavity shows a $\Delta\delta = -4.9$ ppm.[28] There is a significant change in guest position between hemiaminal and imine, most obvious for isopropylamine adducts **17**. The isopropyl group has few degrees of freedom to maximize host:guest interactions, and so it is dependent on the configuration of the asymmetric hemiaminal center. Consequently, there is a large difference in $\Delta\delta$ between the two methyl groups ($\Delta\Delta\delta = 0.5$ ppm): one is deep in the cavity while the other faces the wall. On dehydration, the Me groups are forced into positions similar to each other, and so the $\Delta\delta$ change is less. Isobutylamine adducts **15** are more flexible; the extra methylene unit reduces the effect of the hemiaminal center, so the $\Delta\delta$ between methyl groups is smaller. In the imine, $\Delta\Delta\delta$ is so small that the two signals appear as a triplet. For the unbranched amines, the extra flexibility of the alkyl chain allows the terminal Me to orient itself at an optimal

(28) Menozzi, E.; Onagi, H.; Rheingold, A. L.; Rebek, J., Jr. *Eur. J. Org. Chem.* **2005**, *17*, 3633−3636.

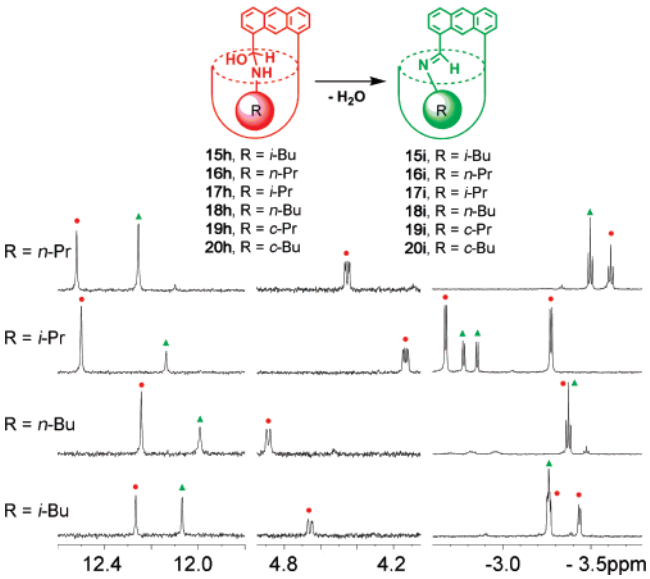

Figure 6. Sections of the ^{1}H NMR spectra (600 MHz, 300 K) obtained upon addition of RNH_2 (10 mM, R = *n*Pr, *i*Pr, *n*Bu, *i*Bu) to a 1.5 mM solution of cavitand **3** in mesitylene-d_{12}. Red circle, hemiaminal intermediate; green triangle, imine product. (a) Downfield region showing benzimidazole proton H_a (see Figure 2); (b) mid-field region showing hemiaminal CH_b; (c) upfield region showing terminal methyl group(s).

position in the cavitand base. On dehydration of *n*-propyl hemiaminal **16h**, there is a small change in $\Delta\delta$ of the terminal CH_3, but for the longer **18h**, the terminal Me's of the hemiaminal and imine show the same chemical shift.

The newly created methine hydrogen of the hemiaminal shows variations in both chemical shifts and coupling patterns. For propyl hemiaminals **16h** and **17h**, this CH resides deeper in the cavity ($\Delta\delta$(**16h:18h**) = −0.5 ppm, $\Delta\delta$(**17h:15h**) = −0.55 ppm). The benzimidazole wall can bend inward or outward to accommodate the R group for an optimal fit in the cavity. Small R groups need to be positioned deeper, as they do not fill the space properly, and, in turn, this affects the shift and coupling patterns of the CH. Each methine exists as two doublets, with each showing a 12 Hz vicinal coupling constant to the NH. No coupling is observed to the OH, and the second splitting is due to the two cycloenantiomers of the amide rim. The two diasteromeric methines in the hemiaminals of **16h** and **17h** are affected to a much larger extent ($\Delta\delta$ = 3 and 6 Hz, respectively) than those of the larger **15h** and **18h** ($\Delta\delta$ = 1 Hz), as they are closer to the plane of the amide rim. This effect is also illustrated by the shift of the benzimidazole proton: the shift for the hemiaminals of **16h** and **17h** is very similar, as it is for the larger **15h** and **18h**.

Other amines are capable of forming stabilized hemiaminals. Ethylenediamine **21** and ethanolamine **22** were added to a 1.5 mM solution of cavitand **3** in mesitylene-d_{12}. ^{1}H NMR analysis showed the initial formation of only one complex in both cases, and those NMR spectra are shown in Figure 7. The two complexes are quite similar; there are slight chemical shift changes, but each complex displays the same pattern of peaks. Most notably, the most upfield signal (corresponding to the proton deepest in the cavity) in **23h** shows an integral of 2H and a chemical shift of δ −3.1 ppm, whereas for **24h**, the equivalent signal integrates to 1H and appears farther downfield at δ −2.5 ppm. This suggests that the two peaks correspond to a deeply bound NH_2 and OH group, respectively. At δ 3.6 ppm in each complex, one can find a doublet corresponding to the hemiaminal proton, similar to that observed upon addition of the alkylamines. Evidently, both of these complexes are hemiaminals, as shown by **23h** and **24h** in Figure 7. No other complex is seen upon initial analysis; the equilibrium between noncovalent complex and hemiaminal lies far to the latter in these cases. Over time, additional peaks grow in, but extremely slowly. After 7 days, only 50% of the hemiaminal complexes have dehydrated. After heating to 340 K for 1 h, complete dehydration can be achieved, yielding products that display the mass of imine complexes. The hemiaminals are so long-lived that they can be analyzed by high-resolution mass spectrometry (HRMS). Both complexes showed ions for $M + H^+ - H_2O$ (2114.2449 and 2115.2320, respectively, for products imine **23i** and **24i**), and hemiaminal **24h** was also detected ($M + H^+$ = 2133.2379).

The long lifetimes of the hemiaminals **23h** and **24h** also allow analysis by 2D NOESY experiments. Figure 8 shows sections of the 2D NOESY spectrum of hemiaminal **23h** (see Supporting Information for full spectrum). The downfield peaks belong to the OH and C*H* of the hemiaminal (δ = 4.7 and 3.6, respectively). These peaks show NOE contacts to each other and also to the upfield, shielded peaks. The OH shows a cross-peak with the deeply bound NH_2 (δ = 4.7 to δ = −2.9). The NH_a quartet of the hemiaminal is quite upfield shifted (δ = −0.9) and shows a cross-peak with methine H_b, although not to the O*H*. These cross-peaks strongly suggest an intramolecular hydrogen bond between the OH and deeply bound NH_2 (and, by inference, the OH in **24h**).

This intramolecular H-bond shifts the observed hemiaminal OH peak significantly downfield. OH groups with strong hydrogen bonding are well known to show resonances as far downfield as 10 ppm. If the "initial" position of this OH was 8 ppm, a $\Delta\delta$ = −3.3 ppm (similar to that seen for NH_a in the same spectrum) would give a signal at δ = 4.7 ppm, as seen. The hydrogen bond between OH and OH in the equivalent ethanolamine complex is less strong, and the OH group is shifted upfield. No peak for OH is observable in the ^{1}H NMR, but the 2D NOESY spectrum shows a cross-peak between H_b and a residue at δ 2.4, obscured by free amine. The weaker H-bond causes a 2 ppm difference in the location of the OH signal.

Both of the complexes **23h** and **24h** are very stable, and 2 h heating at 70 °C was necessary for complete dehydration. The products of this dehydration were expected to be the cyclic aminal/carbinolamine, but this proved not to be the case. ^{1}H NMR analysis shows the presence of two species in the ethylenediamine spectrum in a ratio of 2:1 (Figure 9). The major product is the amino-imine species **23i** with an NH_2 group near the cavitand base. The minor product is the cyclic aminal **23a**, which is in equilibrium with the acyclic imine. In the case of ethanolamine, the cyclic product is not seen, and only hydroxy-imine **24h** is present. The five-membered ring formed in the cyclic aminal product is too small to effectively occupy the cavity when covalently attached to the anthracene arm. The more nucleophilic NH_2 group is more favorable toward cyclization than the OH, and so a small amount of aminal is seen.

Larger amines were also capable of forming imines, but their reaction profile was somewhat different. Here, the addition of either cyclohexylmethylamine or adamantylmethylamine did not cause an immediate folding of the cavitand around the amine.

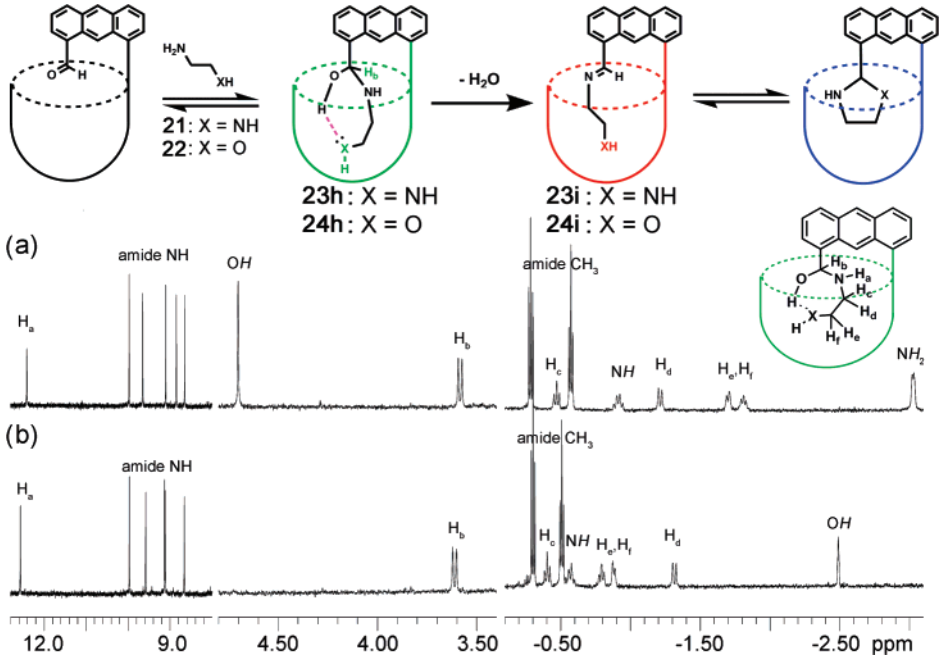

Figure 7. Sections of the ^{1}H NMR spectra (600 MHz, 300 K) obtained upon addition of (a) ethylenediamine **21** and (b) ethanolamine **22** to a 1.5 mM solution of cavitand **3** in mesitylene-d_{12}.

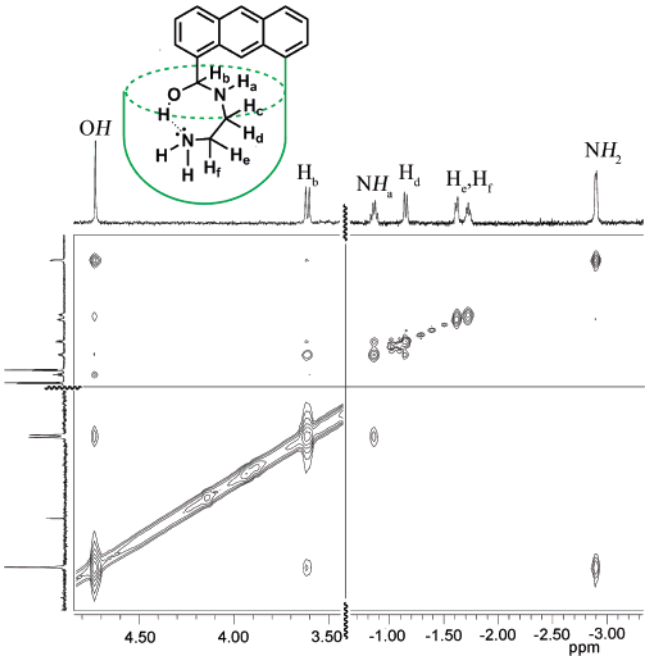

Figure 8. 2D NOESY spectrum (600 MHz, 300 K, 300 ms mixing time) of the hemiaminal **23h** formed by addition of ethylenediamine to a 1.5 mM solution of cavitand **3** in mesitylene-d_{12}.

Weak complexation of a guest species was observed, but sharp peaks for folded cavitand were not. Over time, however, the signals sharpened and a single, well-defined complex was formed: the corresponding imine (as corroborated by MS analysis). During the reaction, no peaks for hemiaminal were seen. The assumption can be made that the initial nucleophilic addition step occurs on unfolded cavitand and binding occurs only at the end of the reaction; hence, the process is similar to the "intermolecular" control.

For a true mimic of the intermolecular reaction, an alternative process is needed. Addition of *n*-hexylamine to **3** in toluene (a competitive solvent) leads to a different product than observed previously. No upfield peaks are seen, but new cavitand peaks grow in over time, as can be seen in Figure 10. The product is an imine, as confirmed by HRMS, but the *n*-hexylimine group is a sufficiently poor guest to be excluded by toluene solvent and exists in the *extroverted* position. It is also notable that no upfield shift occurs for the amide methyl groups (*vide supra*). The reaction is first-order in both cavitand and amine and second-order overall. The kinetic data are tabulated in the Supporting Information. A linear increase in initial rate was observed over a range of concentrations of amine, indicating first-order dependence on amine. The dehydration step is evidently uncatalyzed or aided by the relatively close amide groups of the cavitand; another molecule of amine is not involved in the rate equation. Again, this process occurs by steady-state kinetics, and no hemiaminal can be observed in the reaction.

The extroverted nature of this imine can be easily confirmed by its reaction with an excess of a different amine. Aldehyde **3** (1.5 mM) was exposed to 4 mM *n*-hexylamine and left overnight for complete reaction. The mixture was then exposed to 15 mM isobutylamine. The pseudo first-order rate constant of transimination was $k = 0.14 \times 10^{-3}$ min^{-1}. In contrast, reaction of 1.5 mM introverted *n*-propylimine **16i** with 15 mM isobutylamine gave a transimination rate of $k = 0.0016 \times 10^{-3}$ min^{-1}, a 100-fold reduction in reaction rate. The encapsulation of the imine confers a significant barrier to nucleophilic attack not present in extroverted imine **25**.

III. Mechanistic Details. The stabilization of the hemiaminals seen in the previous section is quite unprecedented; what causes this stability? The relative stability of the hemiaminals can be quantified by measuring the rate of dehydration of each observed species. The rate profile of the reaction of ^{i}BuNH$_2$ with cavitand **3** is shown in Table 2, along with a depiction of the presumed mechanism. The reaction does not follow steady-state kinetics (as the intermolecular counterpart does); rather, the concentration of hemiaminal builds up and declines over time. After a small

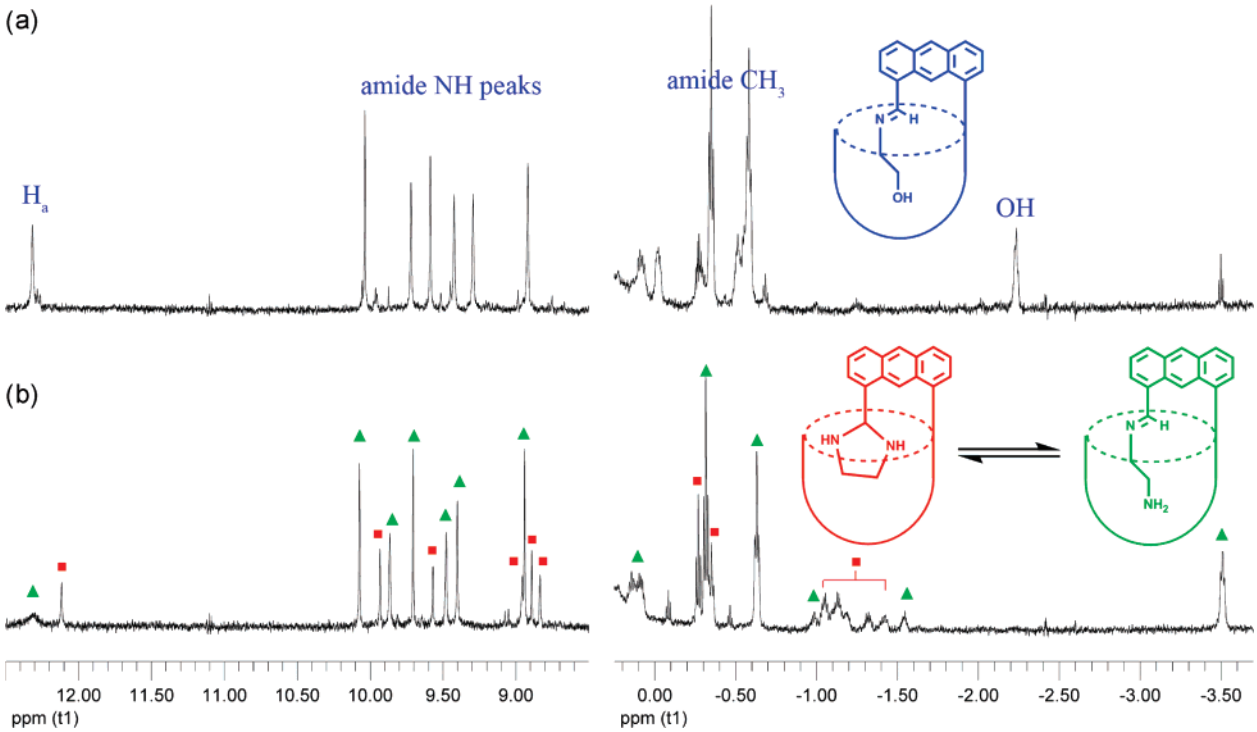

Figure 9. Sections of the ^{1}H NMR spectra (600 MHz, 300 K) obtained upon addition of (a) ethanolamine and (b) ethylenediamine to a 1.5 mM solution of cavitand **3** in mesitylene-d_{12} and heating at 70 °C for 4 h.

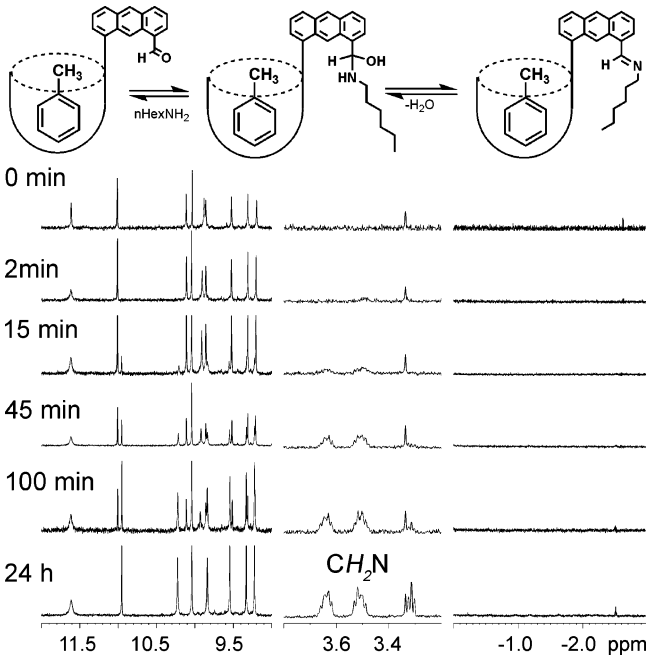

Figure 10. Sections of the ^{1}H NMR spectra (600 MHz, 300 K) obtained over time upon addition of *n*-hexylNH$_2$ (13 mM) to a 1.5 mM solution of cavitand **3** in toluene-d_8.

period of time (<5 min), the rapid formation of hemiaminal from noncovalent complex reaches equilibrium, and the rate of dehydration to imine can be determined. In each case, first-order kinetics is observed, indicating that the dehydration is not catalyzed by free amine base. The eight amines can be split into three similar groups for analysis: α-unsubstituted amines **8**, **10**, and **11**; α-substituted amines **9**, **12**, and **13**; and amines with extra H-bonds **21** and **22**. The H-bonded hemiaminals **23h** and **24h** show the slowest dehydrations, with half-lives of 59 and 94 h, respectively. Linear hemiaminals **15h**, **16h**, and **18h** all show much more rapid dehydration rates, with $t_{1/2} \approx 30$ min. The α-substituted hemiaminals **17h**, **19h**, and **20h** have intermediate dehydration rates, approximately 4−10 times slower than for the α-unsubstituted amines.

There are three components to the hemiaminal stability: the stabilization of the tetrahedral intermediate by the secondary amides on the cavitand rim, the transition barrier conferred by the need to reorganize the cavitand upon dehydration, and an intramolecular H-bond present for amines **21** and **22**. The binding event positions the amine in close proximity with the introverted aldehyde group, and the initial addition reaction becomes practically intramolecular. The newly formed hemiaminal is positioned at the cavitand rim; the organized amide seam is capable of providing hydrogen bonds (and enthalpic stabilization) to the newly formed OH, NH groups. This does not, however, explain the difference in stability between the α-unsubstituted and α-substituted hemiaminals—the first-order dehydration of primary hemiaminals should be the same. The difference comes from the requirement that the reactions take place in a *confined space*. Figure 6 showed the NMR evidence for the repositioning of the R group inside the cavity when going from hemiaminal to imine; this reorganization of the cavitand as a whole contributes to the barrier for dehydration. The α-substituted hemiaminals **17h**, **19h**, and **20h** are significantly less flexible than the linear cases. To avoid steric hindrance between bound R group and the cavitand wall, the cavitand as a whole must distort. Similar cavitands and capsules are capable of "breathing" to allow guest movement,[29] and although the

(29) (a) Scarso, A.; Onagi, H.; Rebek, J., Jr. *J. Am. Chem. Soc.* **2004**, *126*, 12728−12729. (b) Heinz, T.; Rudkevich, D. M.; Rebek, J., Jr. *Angew. Chem., Int. Ed.* **1999**, *38*, 1136−1139. (c) Grotzfeld, R.; Branda, N.; Rebek, J., Jr. *Science* **1996**, *271*, 487−489. (d) Shivanyuk, A.; Rebek, J., Jr. *Chem Commun.* **2001**, 2424−2425.

Table 2. Kinetic Data for the Dehydration of Isobutylamine Hemiaminal (graph) and Various Other Hemiaminal Intermediates (table)

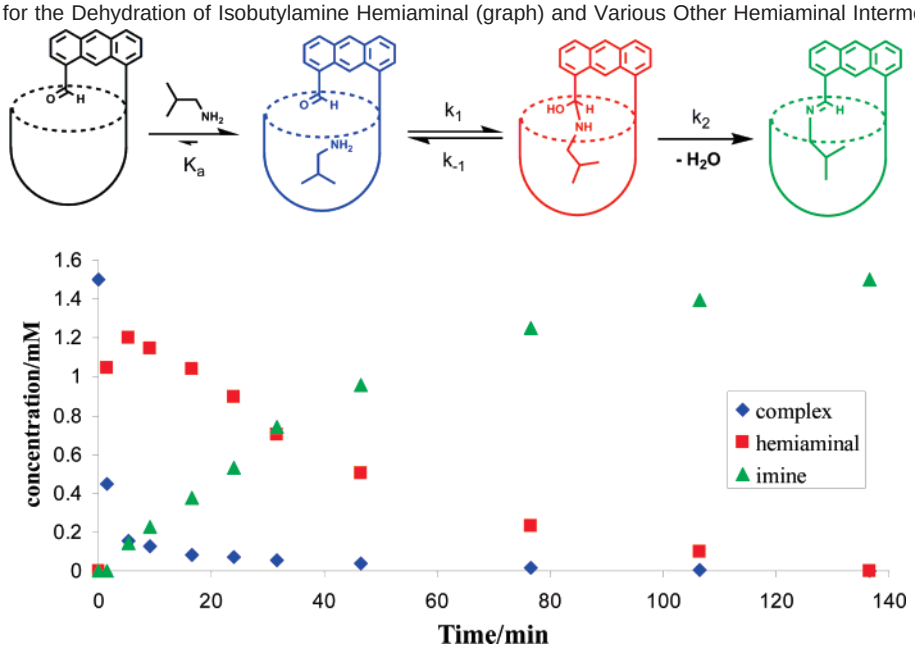

hemiaminal	k_2 (10^{-3} min^{-1})	$t_{1/2}$ (min)	$\Delta G^{\ddagger}$ (kcal mol^{-1})
i-BuNH_2 (**15h**)	26	27	22.2
n-PrNH_2 (**16h**)	15	47	22.5
i-PrNH_2 (**17h**)	5.1	135	23.2
n-BuNH_2 (**18h**)	35	20	22.0
c-PrNH_2 (**19h**)	3.1	221	23.4
c-BuNH_2 (**20h**)	1.7	410	23.8
$HOCH_2CH_2NH_2$ (**24h**)	0.2	3520	25.1
$H_2NCH_2CH_2NH_2$ (**23h**)	0.12	5640	25.5

energetic differences are small (~1 kcal mol^{-1}), they cause a significant (~10-fold) barrier to dehydration.

The long lifetime of the hemiaminals from ethylenediamine and ethanolamine is due to the intramolecular hydrogen bond. Dehydration removes the beneficial hydrogen bond between OH and the electron-rich terminal group and leaves a Coulombic repulsion at the base of the cavity. The barriers to dehydration are shown in Table 2. There is a 3 kcal mol^{-1} difference in the dehydration barrier between ethylenediamine and *n*-propylamine. In addition, the five-membered ring formed by cyclization is too small to adequately occupy the cavity (as shown by the dominance of imine vs aminal product). These disadvantages create a barrier to dehydration that the molecule is slow to cross.

The reaction profile above Table 2 indicates the first two steps are equilibria. This is assumed rather than proven, but the reversible nature of the first two steps can be supported by competition experiments. A 1:1 mixture of isobutylamine and *n*-propylamine with **3** showed immediate formation of hemiaminals. The ratio of the two hemiaminals formed is approximately 1:1. Over time, dehydration occurs and imine product builds up (Figure 11). Throughout the reaction, the ratio of hemiaminals **15h** to **16h** *remains constant*, while the buildup of isobutyl imine **15i** occurs faster than that of *n*-propyl imine **16i**. Consequently, the final ratio of **15i** to **16i**, once the reaction is complete, is 10:1, whereas *no selectivity* between the two hemiaminals was observed. The product-determining step in this case is the irreversible dehydration reaction to produce imine. The equilibria preceding that step (complex and then hemiaminal formation) occur much faster than the dehydration. On conversion of isobutyl hemiaminal to product, the equilibria are shifted toward that product, leading to selectivity based upon the rate of dehydration and *not* the molecular recognition event. Indeed, selectivity between the amines is low, whereas selectivity between imine products is significant. The same principle holds for isopropylamine vs *n*-butylamine; here, hemiaminal formation is favored for i$PrNH_2$ over *n*-BuNH_2 by a ratio of 2:1 (see Supporting Information). The significantly slowed dehydration of isopropylhemiaminal **17h** due to reorganization effects leads to the major reaction product being *n*-butylimine **18i**, with a ratio of 5:1.

Conclusion

The biological solution to highly effective catalysis involves macromolecules that use binding forces to stabilize reactive intermediates by both isolating them from the medium and providing beneficial weak interactions. Here, we have shown that these effects can be successfully mimicked in a synthetic environment. Previously undetectable hemiaminal intermediates are stabilized by binding in a deep cavitand. The half-lives of these hemiaminals vary from 30 min to over 100 h at ambient temperature. The nature of the stabilization is a combination of hydrogen bonding to an organized peptide-like framework at the cavitand rim, mechanical isolation from reactive species in the bulk medium, and the introduction of barriers to dehydration provided by fixation in a restricted space (reorganization of the macromolecule and forced intramolecular hydrogen bonding). These factors contribute to substrate binding by enzymes, but the high turnover and rapid reactions in biological systems

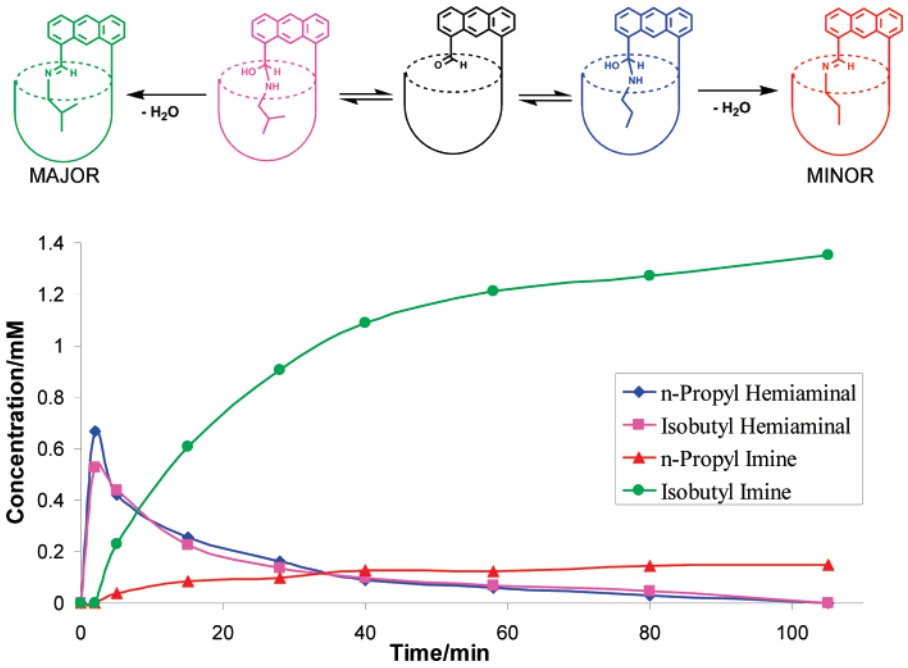

Figure 11. Rate profile of the competing imine formation between equimolar isobutylamine and *n*-propylamine (1.5 mM cavitand **3**, 7.5 mM amines, mesitylene-d_{12}, 300 K).

prevent accurate and direct analysis of reactive intermediates; indirect methods or mutation/alteration of the enzyme are necessary. In this system, the intermediates are sufficiently long-lived to allow study by 2D NMR techniques requiring many hours acquisition. Mechanistic analysis of the final reaction step was performed by direct observation of the conversion of intermediate to product; complex kinetic regression analyses were not necessary to determine the first-order rate constants of dehydration. The analogous "extroverted" reaction was also performed where the addition took place outside the cavitand. This displayed standard steady-state kinetics (as does the intermolecular control); no hemiaminal was observed.

The cavitand also shows strong selectivity based not on binding affinity but on the rate of the product-forming step. A 10:1 ratio of product imines was obtained, while the initial binding ratio was 1:1. The reversible nature of the process allows a relatively featureless cavitand to display strong product selectivity while maintaining the generality of accessible substrates, a most desirable feature when designing reaction promoters. Also, the introversion of an aldehyde group here was merely the first step; by altering the functionality, the system can be used to investigate a variety of reactions. The limitation of this study is the lack of turnover exhibited by the system, but the principle can be expanded to access a new method of accelerated—and possibly catalytic—reactions in an enclosed environment. At the very least, the present study adds an unconventional method for the study of reaction mechanisms.[30]

Experimental Section

General Considerations. ^{1}H NMR, ^{13}C NMR, and 2D spectra were recorded on a Bruker DRX-600 spectrometer with a 5 mm QNP probe. Proton (^{1}H) chemical shifts are reported in parts per million (δ) with respect to tetramethylsilane (TMS, $\delta = 0$) and referenced internally with respect to the protio solvent impurity. Deuterated NMR solvents were obtained from Cambridge Isotope Laboratories, Inc. (Andover, MA) and used without further purification. High-resolution electrospray ionization time-of-flight (ESI-TOF) spectra were acquired on an Agilent ESI-TOF mass spectrometer. Amine guests (>99% purity) and anhydrous solvents were obtained from Aldrich Chemical Co. (St. Louis, MO) and were used as received.

Synthesis of Introverted Aldehyde 3. To a 50 mL sealed tube charged with the diamine **2** (174 mg, 0.094 mmol) and the dialdehyde **4** (22 mg, 0.094 mmol) was added 1,4-dioxane (0.8 mL). Immediately, the tube was soaked into a preheated oil bath (100 °C). After being stirred for 24 h, the reaction mixture was allowed to cool to ambient temperature, and the volatiles were evaporated off. The residue was purified by silica gel column chromatography (CH_2Cl_2/EtOAc = 20/1 to 9/1) to afford **3** as a yellow solid (124 mg, 64% yield): ^{1}H NMR ($CDCl_3$, 600 MHz) δ 11.8 (s, 1H), 10.5 (s, 1H), 10.4 (s, 1H), 9.87 (s, 1H), 9.82 (s, 1H), 9.34 (s, 1H), 9.21 (s, 1H), 8.77 (s, 1H), 8.68 (s, 1H), 8.58 (s, 1H), 8.30 (d, J = 8.4 Hz, 1H), 8.13 (dd, J = 7.2 Hz, 1.8 Hz, 1H), 8.05 (d, J = 7.2 Hz, 1H), 7.99 (s, 1H), 7.85 (s, 1H), 7.81 (s, 1H), 7.71 (s, 1H), 7.69 (dd, J = 8.4 Hz, 1.8 Hz, 1H), 7.63 (s, 1H), 7.55 (s, 1H), 7.48 (s, 1H), 7.44 (s, 1H), 7.43 (m, 1H), 7.29 (s, 2H), 7.244 (s, 1H), 7.236 (s, 1H), 7.224 (s, 1H), 7.217 (s, 1H), 7.19 (s, 1H), 7.157 (s, 1H), 7.151 (s, 1H), 5.78 (t, J = 8.4 Hz, 1H), 5.76 (t, J = 8.4 Hz, 1H), 5.74 (t, J = 8.4 Hz, 1H), 5.66 (t, J = 8.4 Hz, 1H), 2.51−2.20 (m, 14H), 1.49−1.19 (m, 81H), 1.08 (t, J = 7.8 Hz, 3H), 0.91−0.87 (12H, m), 0.62 (t, J = 8.4 Hz, 3H), 0.31 (t, J = 8.4 Hz, 3H); ^{13}C NMR ($CDCl_3$, 150 MHz) δ 192.9 (*C*HO), 175.5, 174.5, 174.2, 172.8 (two peaks are overlapped), 172.2, 157.4, 156.3, 155.4, 155.0, 154.7, 154.6, 154.3, 151.7, 150.7, 150.6, 150.2, 149.9, 149.6, 149.1, 140.5, 138.4, 135.8, 135.51, 135.48, 135.33, 135.29, 134.9, 132.3, 132.0, 131.74, 131.71, 130.8, 130.6, 130.2, 129.5, 128.7, 128.5, 128.2, 127.9, 127.8, 127.1, 125.9, 125.0, 124.6, 124.1, 123.9, 123.4, 122.9, 122.7, 121.6, 121.4, 121.0, 119.1, 117.3, 116.9, 116.2, 116.0, 113.1, 106.5, 33.6, 33.33, 33.27, 33.0, 32.8, 32.3−32.1 (many peaks are overlapped), 31.9, 30.6, 29.9−29.7 (many peaks are overlapped), 29.4, 28.10, 28.07, 22.7, 14.1, 10.7, 10.0, 9.53, 9.10; HRMS (ESI, *m/z*, MH^+) calcd for $C_{130}H_{159}N_8O_{15}$ 2072.1919, found 2072.1859.

General Procedure for Imine Formation. Aldehyde **4** (1.8 mg, 9 × 10^{-4} mmol) was dissolved in mesitylene-d_{12} (600 μL) and added to a 5 mm high-field NMR tube. Amine (10−15 mM final solution, mesitylene-d_{12}) was added via syringe, the NMR tube shaken to allow

(30) Rebek, J., Jr. *Tetrahedron* **1979**, *35*, 723.

mixing, and the mixture analyzed by ^{1}H NMR at set time intervals. The temperature of the reactions was maintained at 300 K throughout the analysis. The relative concentration of the various species was determined by the integration of suitable peaks.

Procedure for NOESY/EXSY Experiments. The NOESY spectra were recorded at 300 K at 600 MHz with the phase-sensitive NOESY pulse sequence supplied with the Bruker software. Each of the 512 F1 increments was the accumulation of 40 scans with a 300 ms mixing time. The MestreC program (Mestrelab Research, Santiago de Compostela) was used to analyze the spectra. Before Fourier transformation, the FIDs were multiplied by a 90° sine square function in both the F2 and the F1 domains. 1K×1K real data points were used, with a resolution of 1 Hz/point. For EXSY analysis, two spectra were taken sequentially, first with 300 ms mixing time and then with 0 ms mixing time. The magnetization transfer rate constants, k_1 and k_{-1}, were calculated using the EXSYCALC program (Mestrelab Research).[19] The rate constant k is the sum of the two dependent magnetization transfer rate constants k_1 and k_{-1} obtained from the calculations, an approximation due to the system being in equilibrium.[21] $\Delta G^{\ddagger}$ was obtained using the Eyring equation.

$$A \underset{k_{-1}}{\overset{k_1}{\rightleftharpoons}} B$$

$$k = k_1 + k_{-1}$$

$$k = \kappa(k_B T/h)\, e^{-\Delta G^{\ddagger}/RT}$$

Acknowledgment. We are grateful to the Skaggs Institute and the National Institutes of Health (GM 27932) for financial support. R.J.H. and T.I. are Skaggs Postdoctoral Fellows. We also thank Drs. Laura Pasternack and Dee-Hua Huang for assistance with NMR experiments.

Supporting Information Available: ^{1}H NMR spectra of all products and intermediates, HRMS data of all imine products, 2D NMR data, and tabulated kinetic analysis. This material is available free of charge via the Internet at http://pubs.acs.org.

JA0759343